Enhanced photovoltaic response by incorporating polyoxometalate into a phthalocyanine-sensitized electrode

Yaobin Yang,[ab] Lin Xu,*[a] Fengyan Li,[a] Xiguang Du*[a] and Zhixia Sun[a]

Received 8th June 2010, Accepted 22nd July 2010
DOI: 10.1039/c0jm01812k

A photovoltaic electrode material consisting of cobalt tetraaminophthalocyanine (CoTAPc) and Dawson-type phosphomolybdate (P_2Mo_{18}) was fabricated through the layer-by-layer (LbL) assembly method. The film electrode was characterized by UV–vis spectroscopy, IR spectroscopy, X-ray photoelectron spectroscopy (XPS), atomic force microscopy (AFM), and photoelectrochemical measurements. Photovoltaic measurement of the film electrode under light irradiation of 365 nm demonstrated that the P_2Mo_{18}/CoTAPc composite film electrode exhibits higher photocurrent and power conversion efficiency (η) than the phthalocyanine-only electrode, furthermore the increased photocurrent of $(P_2Mo_{18}/CoTAPc/PSS/PAH)_5$ is not equal to the direct photoresponse addition of P_2Mo_{18} and CoTAPc. Based on the results of fluorescence quenching measurements, the enhanced photovoltaic effect should be attributed to the occurrence of the photoinduced electron transfer between CoTAPc and POM, which increases the efficient dissociation of excited electron–hole pairs (excitons). The present research represents the first example of enhancing the photovoltaic response of organic photovoltaic materials by the assistance of polyoxometalates.

1. Introduction

Development of promising photovoltaic materials has attracted considerable attention because of the important demands of low-cost production and high efficiency in solar energy conversion.[1] Recently there has been much interest in the photovoltaic properties of organic pigments due to their favorable optical absorption in the UV–vis region of the solar spectrum and their potential application as an inexpensive material for solar cells.[2] Much effort has been dedicated to the discovery of cheaper and more efficient organic pigments for application in photovoltaic devices.[3–5] Since light absorption leads to the generation of excitons in an organic photovoltaic device, the efficient dissociation of strongly bound excitons into free charge carriers and the subsequent charge transfer should be crucial factors in obtaining substantial energy conversion efficiencies. Thus, the enhancement of photovoltaic response by assistance of a secondary molecule is a significant strategy for developing photovoltaic materials based on organic pigments.

Metal phthalocyanines (MPc's), by virtue of their highly delocalized cyclic π-electron systems, show intense absorption in the UV–vis region of solar spectrum and hence have become suitable candidates for research into low-cost organic photovoltaic devices.[6] Recent progress in dye-sensitized solar cells based on phthalocyanine molecules offered an opportunity for achieving the photovoltaic application of phthalocyanine dyes.[7] However, the solar energy conversion efficiency of phthalocyanine dyes is lower than some inorganic photovoltaic materials. Thus the enhancement of photovoltaic response is still a desire for realizing effective utilization of MPc films. It is well-known that high mobility of the excited electrons can reduce the recombination of electrons and holes, which could enhance the photovoltaic response of MPc's. Thus, an intelligent strategy is to incorporate an electron accepting medium into the MPc film for facilitating the generation of charge carriers and tailoring the charge transport properties. To satisfy this demand, the layer-by-layer (LbL) self-assembly technique relying on electrostatic absorption of oppositely charged species has been developed as a simple and efficient approach for the construction of nanocomposite films. This method could have the advantage of controlling morphology, structure and film thickness at molecular-level.

Polyoxometalates (POMs), a class of metal–oxygen cluster compound having remarkable structural diversity and chemical composition variety, have shown unique physicochemical properties and are used in various applications.[8,9] In particular, POM anions are a kind of good electron acceptor and have the ability to promote electron transfer rate of the semiconductor conduction band (CB) by trapping photogenerated electrons. Therefore, the incorporation of POMs into phthalocyanine films may facilitate photogenerated electron transfer and retard exciton recombination. To our knowledge, the combination of POMs with MPc's to improve photoelectrochemical performance has been virtually unexplored so far.

Recently, our group has been interested in the assembly of POMs and MPc's composite films to investigate their nonlinear optical properties[10] and electrocatalytic behavior.[11,12] The research demonstrated an obvious promotion of their functional properties by the synergic effect of POMs. As an extension of our work, herein, we fabricated a photosensitized electrode consisting of CoTAPc and P_2Mo_{18} by the LbL self-assembly technique and investigated its photovoltaic properties. In such a fabrication, the surface of a CoTAPc nanoparticle can be fully coated with a P_2Mo_{18} molecule layer. Further, we observed that

[a]*Key Laboratory of Polyoxometalates Science of Ministry of Education, College of Chemistry, Northeast Normal University, Changchun, 130024, P.R. China. E-mail: linxu@nenu.edu.cn; xgdu@nenu.edu.cn; Fax: +86 431 8509 9668; Tel: +86 431 8509 9668*
[b]*JiLin Institute of Chemical Technology, JiLin City, 132073, P.R. China*

photoinduced charge transfer interactions could occur at the CoTAPc–P_2Mo_{18} interface of the multilayer films, so that their photovoltaic response was obviously enhanced.

2. Experimental

2.1. Materials

Dawson-type polyoxometalates of P_2Mo_{18} and cobalt tetraaminophthalocyanine (CoTAPc) were prepared according to the literature method.[13,14] These compounds were identified by UV–vis adsorption spectra, elemental analysis and IR spectra. 3-Aminopropyltriethoxysilane (APS), poly(styrenesulfonate) (PSS; MW 70 000) and poly(allylamine hydrochloride) (PAH; MW 70 000) were purchased from Aldrich and were used without further treatment. Their chemical structures are shown respectively in Fig. 1. Quartz wafers were used for UV–vis spectroscopy, silicon wafers for atomic force microscopy (AFM) imaging and CaF_2 wafers for IR spectroscopy. The water used in all experiments was deionized to a resistivity of 18 MΩ.

2.2. Preparation of the multilayer electrode

The fabrication of the multilayer film electrode is schematically illustrated in Fig. 2 and was carried out according to the following steps. Quartz and ITO wafers were cleaned respectively in an 80 °C piranha solution [H_2SO_4 : H_2O_2 (7 : 3, v/v)] and in an H_2O : H_2O_2 : NH_4OH (1 : 1 : 1) bath for 20 min. Then they were rinsed with copious deionized water and dried completely. APS modified substrates (quartz or ITO glass) were immersed in 0.1 M HCl solution to get an amino cation surface. Prior to the deposition of CoTAPc and P_2Mo_{18} in the *N*,*N*-dimethyl formamide (DMF) solution, two layers of polyelectrolyte (PSS/PAH) were deposited to ensure an evenly charged surface and increase the surface charge density of the substrate. The silanized substrates were immersed in PSS solution of 10^{-3} M for 20 min, rinsed with water, and dried under a nitrogen stream. Then the PSS coated substrates were exposed to a PAH solution of 10^{-3} M (containing 1 M NaCl; pH = 2) for 20 min. Multilayers were then built up by alternating 20 min immersions in P_2MO_{18} (10^{-3} M, pH = 2–3), CoTAPc (10^{-4} M, pH = 1–2), PSS and PAH

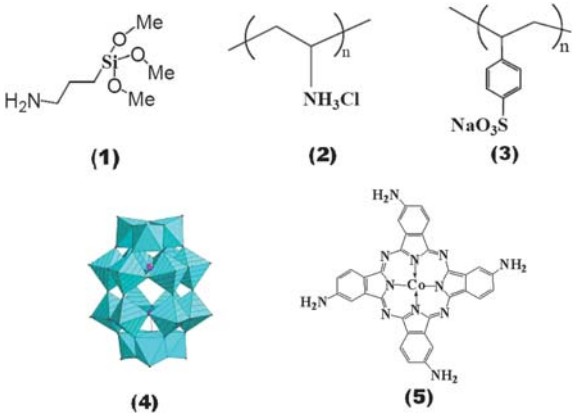

Fig. 1 Structure of 3-aminopropyltrimethoxysilane (1), poly(allylamine hydrochloride) (2), poly(styrenesulfonate) (3), P_2Mo_{18} (4) and cobalt tetraaminophthalocyanine (5).

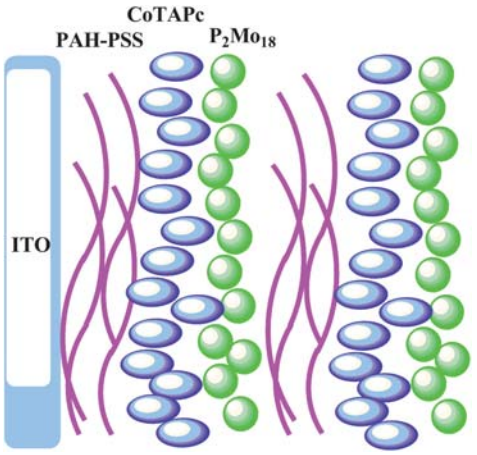

Fig. 2 Schematic representation of the internal layer structure of (P_2Mo_{18}/CoPc/PSS/PAH)} multilayer film self-assembled on a substrate.

solutions, respectively. Water or DMF rinses and nitrogen drying steps were performed after each adsorption step.

2.3. Physical measurements

UV–vis absorption spectra of quartz-supported films were recorded on a 756CRT UV-visible spectrophotometer. FT-IR spectrograms were measured with a Perkin-Elmer 580B infrared spectrophotometer. X-Ray photoelectron spectra (XPS) were measured on silicon wafers using an ESCALAB MK II Surface Analysis System (including X-ray photoelectron spectrometer) with aluminium Kα (1486.6 eV) as X-ray source. A concentric hemispherical analyser (CHA) was used with 50 eV pass energy, and the XPS analysis depth was 3–5 nm. Atomic force microscopy (AFM) images were taken on silicon wafer using a SPVA 400 instrument. The fluorescence spectra were recorded on the FL900/FS920 steady-state fluorescence spectrometer. The photoelectrochemical measurements were carried out on a CH Instrument 660 electrochemical workstation.

2.4. Photoelectrochemical measurements

A specially designed quartz beaker with a three-electrode system was employed in all these experiments. ITO glasses modified with nanocomposite multilayer films were used as working electrodes with an active area of 2 cm^2. The counter electrode was platinum wire, and the reference was a saturated Ag/AgCl electrode. The photoelectrochemical measurements were carried out in 0.1 M Na_2SO_4 solution by a CH Instrument 660 electrochemical workstation. A 5 W UV lamp (main wavelength of 365 nm and radiation intensity of 80 μW cm^{-2}) was used as an irradiation source, and the distance from the source to working electrode was about 5 cm.

3. Results and discussion

3.1. UV–vis spectra characterization of the multilayer films

UV–vis spectroscopy was used to monitor the growth process of the self-assembled films on quartz. The phthalocyanine has characteristic spectral absorption in the UV–vis region. Fig. 3a

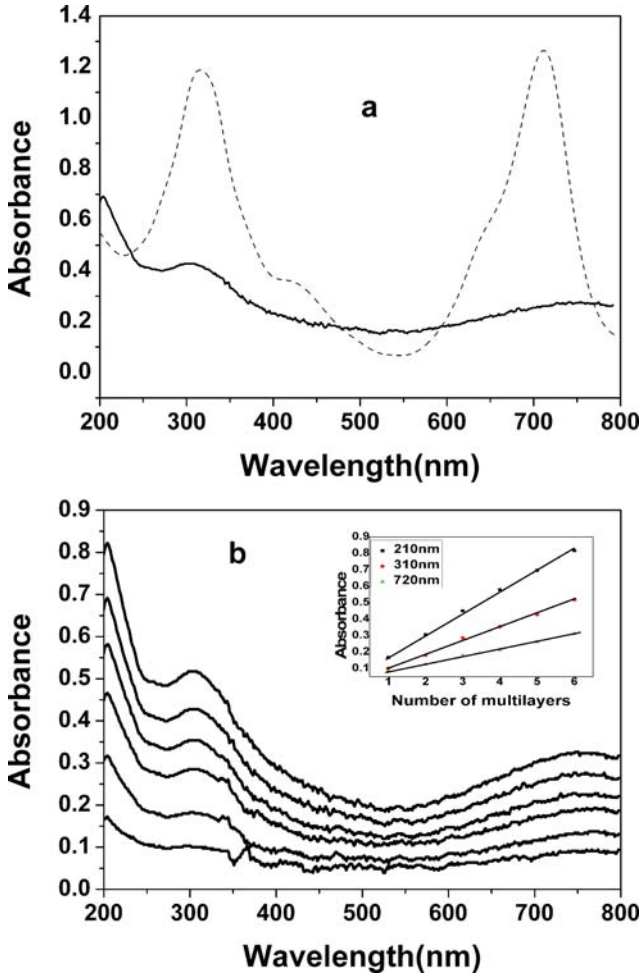

Fig. 3 UV–Vis spectra of cobalt tetraaminophthalocyanine in DMF solution (---) and (CoTAPc/PSS/PAH) films (—) (a) and $(P_2Mo_{18}/CoTAPc/PSS/PAH)_n$ films (n = 1–6) (b) on the precursor film-modified quartz substrate; the inset shows plots of the absorbance values at 210, 310 and 720 nm.

shows the UV–vis absorption spectra of CoTAPc in DMF solution. The absorbance at about 320 nm (B-band) in the UV region arises from the deeper π-levels–LUMO transition. The absorption of the Q-band with a peak at approximately 720 nm is also typical absorption of phthalocyanine materials. The band edge has been assigned to a π–π* transition from the highest occupied molecular orbital to the lowest unoccupied molecular orbital of the phthalocyanine ring through extended Huckel calculations by Schaffer *et al.*[15] The P_2Mo_{18} solution has characteristic absorption peaks, sharp at 210 nm and weak at 310 nm, which are due to the terminal oxygen and bridge oxygen to molybdenum charge transfer transitions, respectively.[16] Fig. 3b shows the UV–vis spectra of the multilayer film of $(P_2Mo_{18}/CoTAPc/PSS/PAH)_n$ (n = 1–6). The characteristic absorption bands at 210 and 310 nm for P_2Mo_{18} and at 720 nm for CoTAPc confirm the incorporation of P_2Mo_{18} and CoTAPc into the composite films without any structural alteration.[16] The Q-band at 720 nm of CoTAPc in the $(P_2Mo_{18}/CoTAPc/PSS/PAH)$ film is very similar to that in the (CoTAPc/PSS/PAH) film, which is broadened and weakened in comparison with CoTAPc (Fig. 3a).

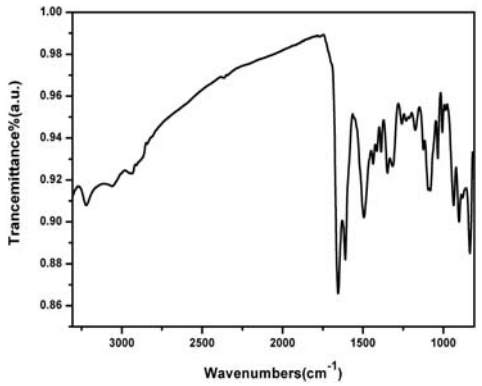

Fig. 4 IR spectrum of $(P_2Mo_{18}/CoTAPc/PSS/PAH)_{10}$ film.

This indicates the occurrence of the same molecular aggregation of CoTAPc in both films.[17] The slight red shift at 720 nm is due to the strong electrostatic attraction between the anionic P_2Mo_{18} and the cationic CoTAPc. The gradual increase of the absorbance in the UV–vis spectra clearly indicates that full layer absorption was attained after each deposition step. In addition, a good linear relationship between the absorbance and the number of P_2Mo_{18}/CoTAPc/PSS/PAH layers (inset plot in Fig. 3b) at 210 nm, 310 nm and 720 nm shows that the P_2Mo_{18} anions and CoTAPc cations are smoothly deposited on each layer of the multilayer.

3.2. IR spectrum

Fig. 4 shows the IR spectrum of the $(P_2Mo_{18}/CoTAPc/PSS/PAH)_{10}$ composite film. The features at 1653, 1606 and 1492 cm^{-1} are associated with the antisymmetric and symmetric stretching vibrations of the C=C and C=N bonds in phthalocyanine molecule, and the five vibration bands at 1083, 1003, 936, 906 and 851 cm^{-1} are assigned to ν_{as}(P–O_a) two peaks, ν_{as}(Mo–O_d), ν_{as}(Mo–O_b–Mo) and ν_{as}(Mo–O_c–Mo) peaks, respectively. These five bands indicate characteristically the Dawson structure of P_2Mo_{18} anions.[18] These infrared spectrum results indicate that both the inorganic P_2Mo_{18} anions and organic phthalocyanine CoTAPc molecules have been incorporated into the multilayer film.

3.3. X-Ray photoelectron spectra (XPS)

The corresponding XPS spectra provide further information for the $(P_2Mo_{18}/CoTAPc/PSS/PAH)_2$ multilayer films, as show in Fig. 5. Although the XPS measurement gives only a semi-quantitative elemental composition, the expected molar ratio of 2 : 18 for P to Mo is also approximately established and the peaks of Mo 3d, Co 2p and N 1s were observed at 232.8 eV, 781.4 eV, 796.2 eV and 399.5 eV, respectively. Table 1 lists the binding energy of various atoms in the CoTAPc film before and after the combination of P_2Mo_{18} measured from the XPS. From Table 1 we can find that the binding energy of N and Co atoms in CoTAPc changed after incorporating POMs. *Ev* of the N 1s increased by 0.6 eV, and *Ev* of the Co 2p3/2 and Co 2p1/2 increased by 0.3 and 0.6 eV, respectively. For the X-ray photoelectron spectra, it is well-known that the binding energy increases with the decreased electronic density around atomic

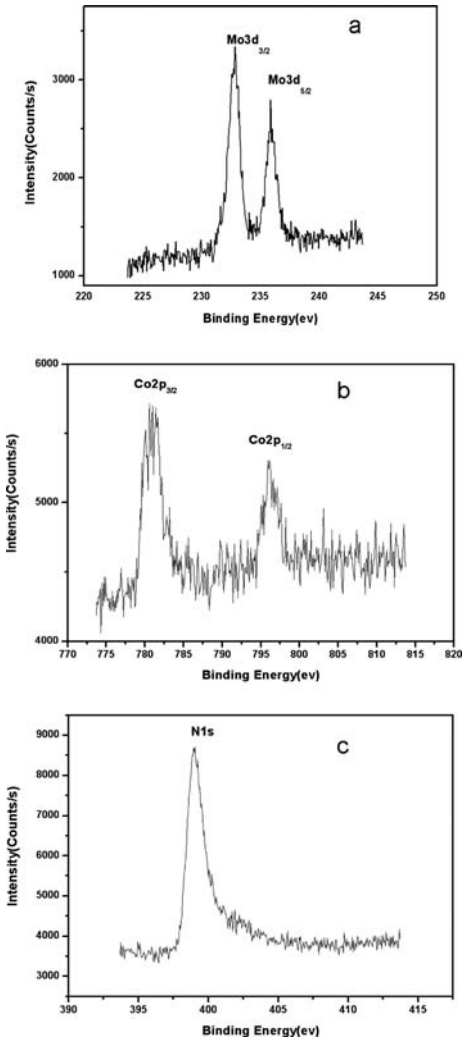

Fig. 5 XPS spectra of the [PSS/PAH/(P_2W_{18}/CoTAPc/PSS/PAH)$_2$] film (a) Mo 3d (b) Co 2p (c) N 1s.

Table 1 Binding energy (*Ev*) of CoTAPC and CoTAPC/P_2Mo_{18} composite film

	N 1s	Co 2p3/2	Co 2p1/2
CoTAPC	398.9	781.1	795.6
CoTAPC/P_2Mo_{18}	399.5	781.4	496.2

nuclear. Since the binding energy of the N 1s and Co 2p increases after the electrostatic association of anionic P_2Mo_{18}, the occurrence of the electron transfer from CoTAPc to P_2Mo_{18} should be considered properly.

3.4. Morphology of the film

AFM can provide detailed information about the surface morphology and homogeneity of the deposited film. Fig. 6 shows AFM images of the (P_2Mo_{18}/CoTAPc/PSS/PAH)$_2$ film. The samples present typical spherical or granular patterns similar to other classes of POM-deposited LbL films and the film surfaces are uniform and smooth; this can be ascribed to the P_2Mo_{18}

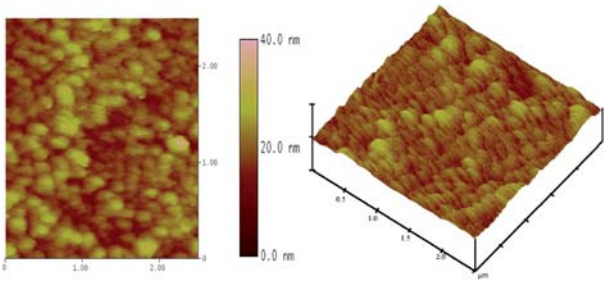

Fig. 6 AFM images of the (P_2Mo_{18}/CoPc/PSS/PAH)$_3$ film on silicon matrix substrate.

aggregating to a certain level because the cationic CoTAPc may reduce the coulombic repulsion of adjacent POM centers.[19] In addition, the vertical grain structure seen in the three-dimensional AFM image of the multilayer surface presents a lot of small protuberant peaks, indicating that the distribution of aggregated nanoclusters is almost uniform. According to the AFM image, the mean surface roughness of the film is *ca.* 1.14 nm, and the film thickness can be estimated from the height of valley-to-peak to be about 3 nm.

3.5. Photoelectrochemical performances

The photocurrent responses of the (P_2Mo_{18}/PAH)$_5$, (CoTAPc/PSS)$_5$ and (P_2Mo_{18}/CoTAPc/PSS/PAH)$_5$ composite films were measured with ITO electrodes. The applied potential was 0.6 V *versus* a Ag/AgCl electrode and the sample was exposed under UV (365 nm) light for 50 s and kept in dark for another 50 s. As shown in Fig. 7, the (P_2Mo_{18}/PAH)$_5$ films show a negligible photocurrent, whereas the other two kinds of film electrodes containing CoTAPc show a rapid and bigger photocurrent as the irradiation is switched on and off. Evidently, the P_2Mo_{18}-only film electrode presents a poor photoresponse with excitation at 365 nm. Therefore, the CoTAPc should be responsible for the photocurrent generation as the cause of the light-to-electric conversion. However, the (P_2Mo_{18}/CoTAPc/PSS/PAH)$_5$ film electrode, incorporated with POMs, shows a stronger photocurrent response than the (CoTAPc/PSS)$_5$ film electrode. The

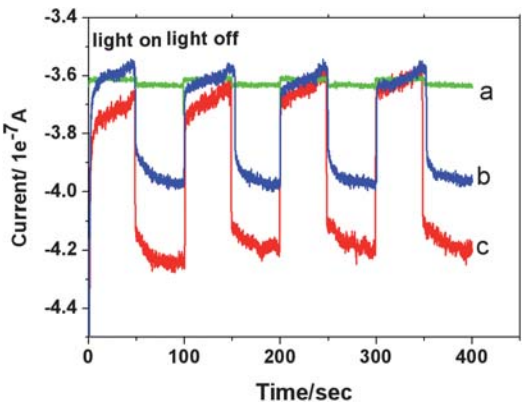

Fig. 7 Photocurrent responses with on-off UV light illumination (applied potential, 0.6 V *versus* Ag/AgCl): (a) (P_2Mo_{18}/PAH)$_5$ film electrode; (b) (CoTAPc/PSS)$_5$ film electrode; and (c) (P_2Mo_{18}/CoTAPc/PSS/PAH)$_5$ film electrode.

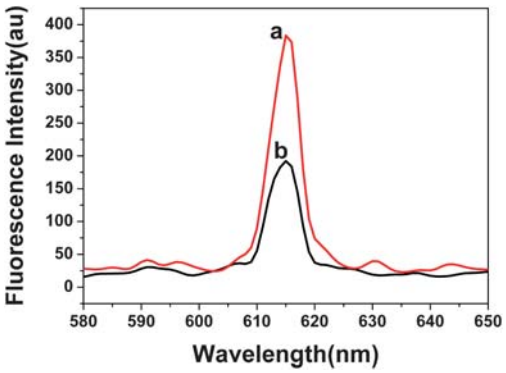

Fig. 8 Fluorescence emission spectra of $(CoTAPc/PSS)_{40}$ films (a) and $(P_2Mo_{18}/CoTAPc/PSS/PAH)_{40}$ films (b).

increased photocurrent of $(P_2Mo_{18}/CoTAPc/PSS/PAH)_5$ is not the simple photoresponse accumulation of P_2Mo_{18} and CoTAPc (see Fig. 7), but a synergic result of the two components. Fig. 8 shows the fluorescence emission spectra of the $(CoTAPc/PSS)_{40}$ film and the $(P_2Mo_{18}/CoTAPc/PSS/PAH)_{40}$ film. Both films have a fluorescence emission band at 615 nm upon excitation at 333 nm. The fluorescence is clearly quenched in the $(P_2Mo_{18}/CoTAPc/PSS/PAH)_{40}$ film, though the position and shape of the band remain the same. The photoinduced electron transfer from the CoTAPc to P_2Mo_{18} clusters should be responsible for the fluorescence quenching.[20] Therefore, such enhancement of the photocurrent can be attributed to strong photoinduced electron transfer interactions at the CoTAPc–P_2Mo_{18} interface in the films. Since the LUMO level of the P_2Mo_{18} is lower than the edge of the CoTAPc conduction band,[21,22] some excited electrons could inject from the CoTAPc to the POM. The energy level and electron-transfer processes are schematically illustrated in Fig. 9. The excited electron transfer can reduce the recombination of electrons and holes in CoTAPc, which results in enhancement of photovoltaic response of CoTAPc. Thus, the P_2Mo_{18}-coated CoTAPc electrode certainly displayed higher photocurrent response than the CoTAPc-only electrode.

To further investigate the photoinduced behavior of $(P_2Mo_{18}/CoTAPc/PSS/PAH)_5$ and $(CoTAPc/PSS)_5$ film electrodes, the *I–V* profiles (Fig. 10) of two kinds of film electrodes illuminated

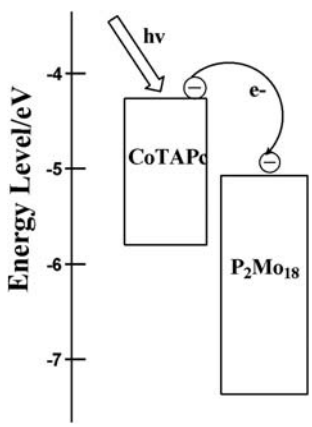

Fig. 9 Energy level and electron-transfer processes diagram of CoTAPc and P_2Mo_{18} molecules.

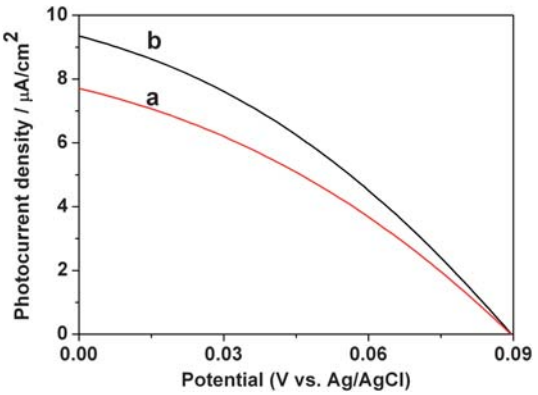

Fig. 10 *I–V* characteristics of (a) $(CoTAPc/PSS)_5$ film electrode, (b) $(P_2Mo_{18}/CoTAPc/PSS/PAH)_5$ film electrode, excited with a UV lamp with an incident light intensity of 80 μW cm^{-2}.

under a 5 W UV lamp (main wavelength of 365 nm and radiation intensity of 80 μW cm^{-2}) were also measured by linear sweep voltammetry. The $(CoTAPc/PSS)_5$ film electrode presents a short-circuit current density (J_{sc}) of 7.7 μA cm^{-2} with an open-circuit voltage (V_{oc}) of 0.09 V, and the fill factor (*FF*) is 32% with a power conversion efficiency (η) of 0.29%. For the $(P_2Mo_{18}/CoTAPc/PSS/PAH)_5$ film electrode, the *I–V* curves show a J_{sc} of 9.1 μA cm^{-2} with an V_{oc} of 0.1 V, a *FF* of 34% and a power conversion efficiency of $\eta = 0.36\%$. The fill factor (*FF*) and power conversion efficiency (η, %) were calculated using the short-circuit current and open-circuit voltage.[23]

$$FF = (JV_{max})/(J_{sc}V_{oc}) \quad (1)$$

$$\eta = (JV_{max})/I_i = FF(J_{sc}V_{oc})/I_i \quad (2)$$

As a result, the $(P_2Mo_{18}/CoTAPc/PSS/PAH)_5$ film electrode exhibits higher *FF* and η than the $(CoTAPc/PSS)_5$ film electrode. The incorporation of P_2Mo_{18} into the CoTAPc-sensitized electrode not only improves photoinduced electron transfer but also decreases the recombination of electrons and holes in CoTAPc, resulting in the enhancement of the power conversion efficiency (η) of CoTAPc. These results are consistent with that of the photocurrent response. While the combination of phthalocyanine and other functional dopants was rarely investigated,[24] the introduction of POMs in phthalocyanine electrodes should be a new strategy to enhance the photovoltaic response.

4. Conclusions

In summary, two kinds of photovoltaic electrodes containing CoTAPc were successfully fabricated through LbL assembly method and their photovoltaic performances were investigated by photocurrent transient measurements and *I–V* profile measurements. The P_2Mo_{18}/CoTAPc composite film electrode showed higher photocurrent response and power conversion efficiency (η) than the CoTAPc-only electrode. This can be attributed to the occurrence of the photoinduced electron transfer between CoTAPc and P_2Mo_{18}, which increases the efficient dissociation of excitons. These results demonstrated that

the introduction of P_2Mo_{18} into a CoTAPc electrode is an effective approach to enhance the photoresponse. The synergic effect of improving photovoltaic response by the combination of POMs and phthalocyanines represents a promising strategy for developing advanced photovoltaic materials and in designing organic photovoltaic devices.

Acknowledgements

The authors are thankful for the financial support from the Natural Science Foundation of China (Grant No. 20731002 and 20971019). This work was also supported financially by the Program for Changjiang Scholars and Innovative Research Team in University and by Science Foundation for Young Teachers of Northeast Normal University (Grant No. 20090403).

Notes and references

1 R. F. Service, *Science*, 2008, **319**, 718–720.
2 B. A. Gregg, *J. Phys. Chem. B*, 2003, **107**, 4688–4698.
3 W. Ma, C. Yang, X. Gong, K. Lee and A. J. Heeger, *Adv. Funct. Mater.*, 2005, **15**, 1617–1622.
4 F. Yang, M. Shtein and S. R. Forrest, *Nat. Mater.*, 2004, **4**, 37–41.
5 M. C. Scharber, D. Mühlbacher, M. Koppe, P. Denk, C. Waldauf, A. J. Heeger and C. J. Brabec, *Adv. Mater.*, 2006, **18**, 789–794.
6 A. M. Saleh, A. K. Hassan and R. D. Gould, *J. Phys. Chem. Solids*, 2003, **64**, 1297–1303.
7 G. D. Sharma, V. S. Choudhary and M. S. Roy, *Sol. Energy Mater. Sol. Cells*, 2007, **91**, 1087–1096.
8 C. L. Hill, *Chem. Rev.*, 1998, **98**, 1–2.
9 D. L. Long, E. Burkholder and L. Cronin, *Chem. Soc. Rev.*, 2007, **36**, 105–121.
10 L. Xu, E. B. Wang, Z. Li, D. G. Kurth, X. G. Du, H. Y. Zhang and C. Qin, *New J. Chem.*, 2002, **26**, 782–786.
11 Y. N. Jin, L. Xu, L. D. Zhu, W. J. An and G. G. Gao, *Thin Solid Films*, 2007, **515**, 5490–5497.
12 Y. B. Yang, L. Xu, B. B. Xu, X. G. Du and W. H. Guo, *Mater. Lett.*, 2009, **63**, 608–610.
13 N. Haraguchi, Y. Okaue, T. Isobe and Y. Matsuda, *Inorg. Chem.*, 1994, **33**, 1015–1020.
14 B. N. Achar, G. M. Fohlen, J. A. Parker and J. Keshavayya, *Polyhedron*, 1987, **6**, 1463–1467.
15 A. M. Schaffer, M. Gouterman and E. Davidson, *Theor. Chim. Acta*, 1973, **30**, 9–30.
16 J. Gong, Y. G. Chen and L. Y. Qu, *Polyhedron*, 1996, **15**, 2273–2277.
17 D. Xie, Y. D. Jiang, Y. G. Ning, J. Z. Jiang, Z. M. Wu and Y. Y. Li, *Mater. Lett.*, 2001, **51**, 1–6.
18 J. F. Garvey and M. T. Pope, *Inorg. Chem.*, 1978, **17**, 1115–1118.
19 L. Cheng and J. A. Cox, *Chem. Mater.*, 2002, **14**, 6–8.
20 B. B. Xu, M. Lu, J. Kang, D. G. Wang, J. Brown and Z. H. Peng, *Chem. Mater.*, 2005, **17**, 2841–2851.
21 A. Hiskia, A. Mylonas and E. Papaconstantinou, *Chem. Soc. Rev.*, 2001, **30**, 62–69.
22 G. Y. Sang, Y. P. Zou and Y. F. Li, *J. Phys. Chem. C*, 2008, **112**, 12058–12064.
23 C. D. Grant, A. M. Schwartzberg, G. P. Smestad, J. Kowalik, L. M. Tolbert and J. Z. Zhang, *Synth. Met.*, 2003, **132**, 197–204.
24 J. Inoue, K. Yamagishi and M. Yamashita, *J. Cryst. Growth*, 2007, **298**, 782–786.

